and Su (2013) built an analytical model of the workspace of a meso-scale hexapod nanopositioner based on the stiffness of flexures and inverse kinematics. Ji et al. (2012) designed a 6DOF nanopositioner and derived a control model based on the stiffness, the comb drive force, and the integrated capacitive displacement sensor. Shi et al. (2014) built a stiffness based analytical control model for a MEMS hexapod nanopositioner. However, there is less work done related to the analysis of applying external loading on a hexapod mechanism.

In this paper, we adopt the Screw Theory to derive a symbolic model of the 6DOF stiffness matrix of the hexapod nanopositioner with respect to the external loading. This macro-scale monolithic hexapod nanopositioner was previously built by the National Institute of Standards and Technology (NIST), USA. The derivation follows a bottom-up procedure, which starts from the three locked actuating stages to the end effector, the center of the top platform. Based on the model, we analyze the relationship between the displacement of the top platform and the external loading. The rest of the paper is organized as follows. Section 2 describes the geometric and material properties of the hexapod platform. Section 3 presents the Screw Theory and the stiffness matrix of single wire flexure. In section 4, we illustrate the topology of the hexapod platform according to the external loading. The analytical model of the external loading is derived and shown with an example. The conclusion is stated in Section 5.

2 KINEMATIC MODEL

As shown in Fig. 1, the hexapod motion stage is composed of three main parts: base stages, struts, and top platform. Three X-Y micro-positioning base stages, which can generate motion in two orthogonal directions, are symmetrically positioned on the base plane.

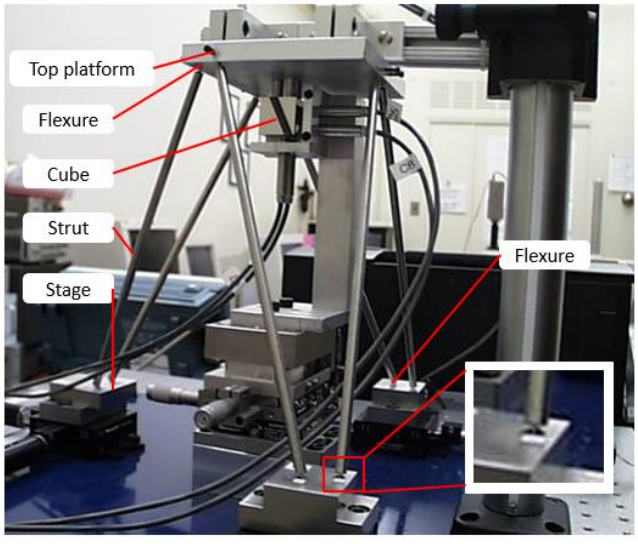

Figure 1: Setting of the 6 DOF NIST hexapod motion stage.

In this study, we consider the linear actuator is rigid enough and it is locked before providing linear motion. We assume the three bottom stages are fully constrained in the plane so that the displacement of the top platform is only caused by the deformation of the compliant parts. As shown in Fig. 2, we build the coordinate system on the center of the top surface of the top platform. The external forces and moments in three directions are applied on the coordinate origin.

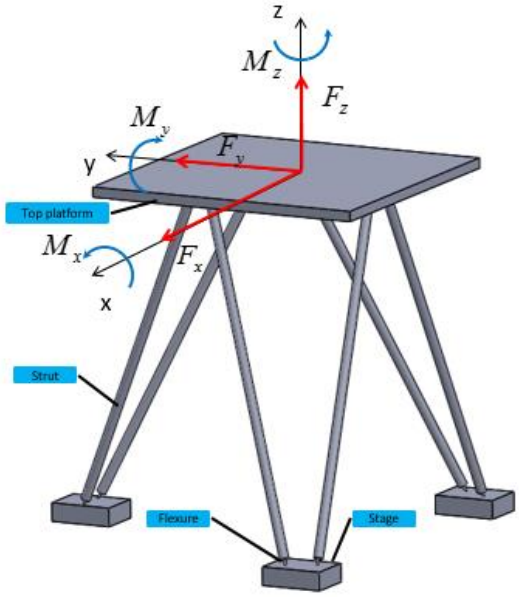

Figure 2: Schematic drawing of the hexapod mechanism

For convenience, we define the following parameters for describing the geometry of the kinematic model. The struts have a total length *L* and diameter *D*, and have a short flexure joint of length l and diameter *d* at each end. Figure 3 shows the geometrical relationship of the twelve points. We denote the position of the six points at the top platform and the six at the base stages by A_i, and by B_i, respectively. The distance between the neighboring intersecting points of the struts at the top platform is C_3. The distance between the non-neighbor intersecting points of the struts at the top platform is C_4. For the base stages, the distance between the neighboring intersecting points of the struts is C_1. The distance between the non-neighboring intersecting points of the struts at the base is C_2. These points on the moving platform and the stages can be described in the global coordinate frame as

$$A_i = [Z(\phi_i)]\begin{Bmatrix} r_a \\ 0 \\ -t \end{Bmatrix}, \quad i = 1,\ldots,6,$$
$$B_i = [Z(\psi_i)]\begin{Bmatrix} r_b \\ 0 \\ -H-t \end{Bmatrix}, \quad i = 1,\ldots,6, \tag{1}$$

where $[Z(\cdot)]$ is the 3-by-3 rotation matrix about the z axis. r_a and r_b are the radii of the strut attachment points (bottom plates in home position). *H* is the height of the hexapod mechanism from the bottom stage to the top plane of the platform and it is derived as the unknown by solving equation $(A_1 - B_1)^T (A_1 - B_1) - L^2 = 0$. *t* is the thickness of the top platform. Angles ϕ_i, and ψ_i, are tabulated in Table 1. All struts are made of aluminum with Young's modulus of elasticity *E*=210 GPa, and Poisson's ratio $\upsilon = 0.28$.

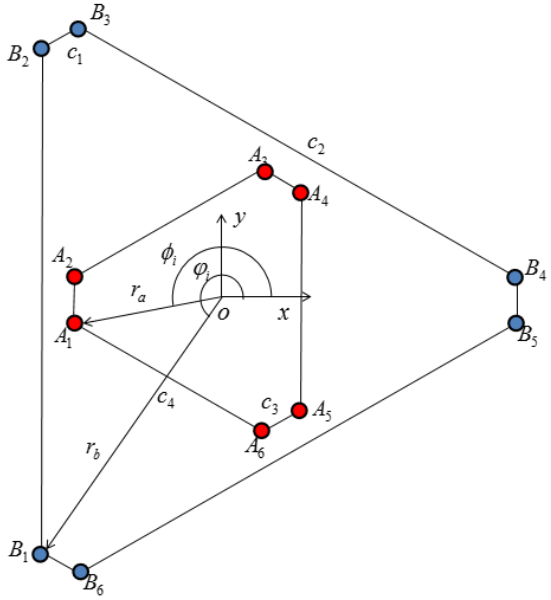

Figure 3: Geometrical layout of the flexure center of the the top platform and the bottom stages.

3 STIFFNESS MATRIX OF WIRE FLEXURE

In order to analyze the impact of the external load applied on the device, we need to determine the relationship between deformation and the loading. Here, we apply the Screw Theory approach to derive the stiffness matrix and analyze the motion of the top platform. This methodology is presented in Su et al. (2011), Su et al. (2012) and Shi (2013). For convenience, a brief description of this approach is given below.

We denote the deformation of a flexure mechanism by a general twist $\hat{T} = (\theta_x, \theta_y, \theta_z, \delta_x, \delta_y, \delta_z)$ and the load is denoted by a wrench $\hat{W} = (F_x, F_y, F_z, W_x, W_y, W_z)$. They are related by,

$$\hat{W} = [K]\hat{T}, \quad \hat{T} = [C]\hat{W}, \quad [C][K] = [I], \tag{2}$$

where [*K*] and [*C*] are six by six stiffness and compliance matrices, respectively.

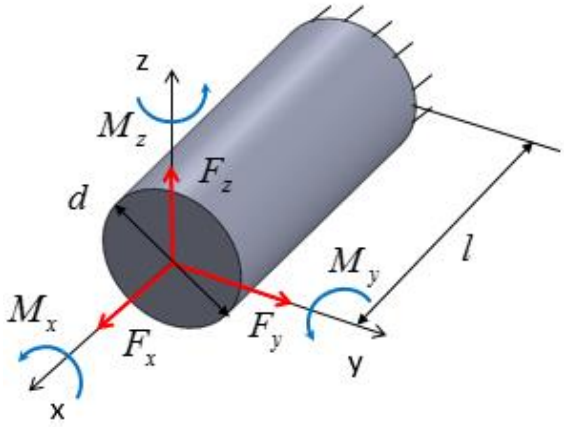

Figure 4: Modeling of a wire flexure based on the Screw Theory

As shown in Fig. 4, a flexure with circular cross section is fixed on one end. The coordinate system is built on the center of the free end. The stiffness matrix of it can be written as

$$[K^w] = \frac{EI_z}{l}\begin{bmatrix} 0 & 0 & 0 & \frac{16}{l^2\eta} & 0 & 0 \\ 0 & 0 & -\frac{6}{l} & 0 & \frac{12}{l^2} & 0 \\ 0 & \frac{6}{l} & 0 & 0 & 0 & \frac{12}{l^2} \\ 2\chi & 0 & 0 & 0 & 0 & 0 \\ 0 & 4 & 0 & 0 & 0 & \frac{6}{l} \\ 0 & 0 & 4 & 0 & -\frac{6}{l} & 0 \end{bmatrix}, \quad (3)$$

where $\eta = d^2/l^2$, $x = 1/2(1+\upsilon)$, are non-dimensional constants determined by the geometries and the material properties. $I_z = \pi d^4/64$ is the area moments of inertia about z axis. *E* is Young's module and $\upsilon = 0.28$ is the Poisson's ratio. After substituting the parameters in Table 1, we obtained the compliance matrix as

$$[C^w] = [K^{\backslash w}]^{-1} = \begin{bmatrix} 0 & 0 & 0 & 1.74E-4 & 0 & 0 \\ 0 & 0 & -2.72E-4 & 0 & 1.36E-4 & 0 \\ 0 & 2.72E-4 & 0 & 0 & 0 & 1.36E-4 \\ 1.43E-5 & 0 & 0 & 0 & 0 & 0 \\ 0 & 7.25E-4 & 0 & 0 & 0 & 2.72E-4 \\ 0 & 0 & 7.25E-4 & 0 & -2.72E-4 & 0 \end{bmatrix}. \quad (4)$$

Table1. Geometric dimensions of the hexapod mechanism

$r_a = 64.29mm, r_b = 138.92mm, t = 13.2mm, H = 215.33mm, L = 240mm, l = 4mm$
$D = 6mm, d = 1.3mm, c_1 = 20mm, c_2 = 230mm, c_3 = 20mm, c_4 = 100mm$
$\phi_1 = 189^\circ, \phi_2 = 171^\circ, \phi_3 = 69^\circ, \phi_4 = 51^\circ, \phi_5 = -51^\circ, \phi_6 = -69^\circ$
$\psi_1 = 236^\circ, \psi_2 = 124^\circ, \psi_3 = 116^\circ, \psi_4 = 4^\circ, \psi_5 = -4^\circ, \psi_6 = -116^\circ$

4 STIFFNESS ANALYSIS OF THE NIST HEXAPOD NANOPOSITIONER

In this section, we derive the stiffness matrix based on the topology of the mechanism according to the Screw Theory.

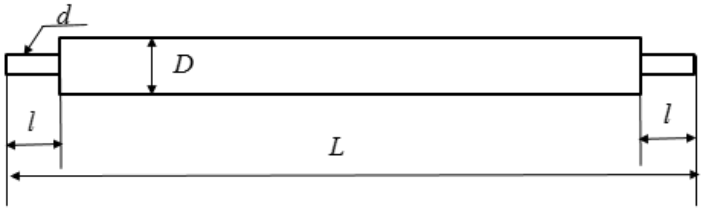

Figure 6: Schematic drawing of one strut.

The compliance matrix of each wire flexure is denoted by [C^w], shown in Eq. (3). The compliance matrix of each strut is denoted as [C^s]. As shown in Fig. 6, the strut is modeled as a serial chain of a cylindrical rod with diameter *D* and two wire flexure joints with diameter *d* at both ends. By the equation of serial flexure chain, we derive mathematically the overall compliance matrix of a serial flexure chain as,

$$[C^s] = \sum_{i=1}^{3} [Ad_i][C_i][Ad_i]^{-1}, \tag{5}$$

where [Ad_i] is the so-called 6-by-6 adjoint transformation matrix,

$$[Ad_i] = \begin{bmatrix} R & 0 \\ DR & R \end{bmatrix}. \tag{6}$$

Here [*R*] is a 3-by-3 rotation matrix. [*D*] is the skew-symmetric matrix defined by a translational vector *d*. By Eq. (3) and Table 1, we obtain [C_1] = [C_3] = [C^w]. As shown in Fig. 6, the compliance of the compliant cylindrical rod [C_2] is obtained by substituting the diameter *D* and length $L-2l$ into Eq. (3). The three adjoint matrices are defined by

$$\begin{aligned}[R_1] = I, d_1 = (0,0,0),\\ [R_2] = I, d_1 = (-l,0,0),\\ [R_3] = I, d_1 = (-L+l,0,0).\end{aligned} \tag{7}$$

Again, we can obtain the stiffness matrix by substituting the parameters in Table 1.

$$[K^s] = [C^s]^{-1} = \begin{bmatrix} 0 & 0 & 0 & 1.34E4 & 0 & 0 \\ 0 & 0 & -3.11E1 & 0 & 2.59E-1 & 0 \\ 0 & 3.11E1 & 0 & 0 & 0 & 2.59E-1 \\ 2.70E3 & 0 & 0 & 0 & 0 & 0 \\ 0 & 7.19E3 & 0 & 0 & 0 & 3.11E1 \\ 0 & 0 & 7.19E3 & 0 & -3.11E1 & 0 \end{bmatrix}. \tag{8}$$

The struts are connected to the top platform in parallel. The overall stiffness matrix of six parallel flexure chain is calculated as

$$[K] = \sum_{i=1}^{6} [Ad_i][K^s][Ad_i]^{-1}, \tag{9}$$

where the adjoint matrices are the coordinate transformation of each strut. As shown in Fig. 7, the coordinate transformation of No.4 and No. 5 struts to the center of the top platform is calculated by three steps, so the adjoint matrices are defined by the multiply of three matrices. No. 6 and No. 2 struts are obtained by a rotation of No.4. No. 1 and No.3 struts are obtained by rotation of No. 5. Therefore, the adjoint matrices of these struts can be written as.

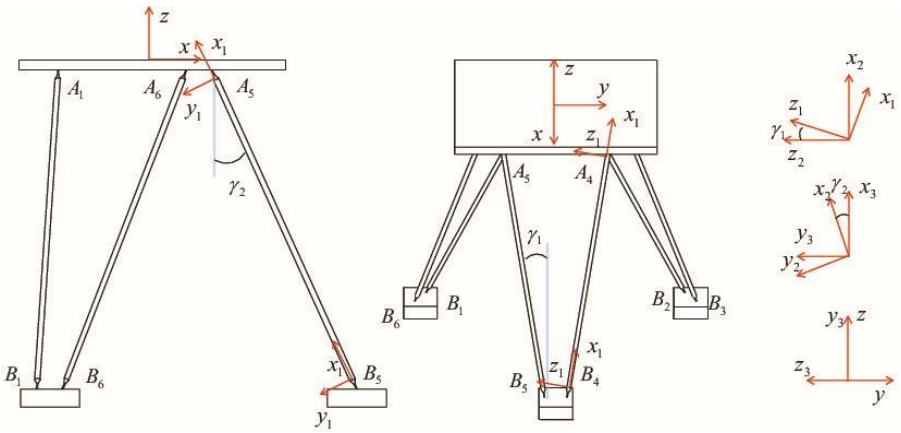

Figure 7. Coordinate transformations of the derivation

$$
\begin{aligned}
&[Ad_4] = [Ad_4^3][Ad_4^2][Ad_4^1],\\
&[Ad_6] = [Ad_6^4][Ad_4],\\
&[Ad_2] = [Ad_2^4][Ad_4],\\
&[Ad_5] = [Ad_5^3][Ad_5^2][Ad_5^1],\\
&[Ad_1] = [Ad_1^4][Ad_5],\\
&[Ad_3] = [Ad_3^4][Ad_5],
\end{aligned}
\tag{10}
$$

where the rotation matrices and translational vectors of joint matrices are defined by

$$
\begin{aligned}
&[R_4^1] = [Y(\gamma_1)], d_1^1 = (0,0,0),\\
&[R_4^2] = [Z(\gamma_2 + \pi/2)], d_1^2 = (0,0,0),\\
&[R_4^3] = [X(\pi/2)], d_1^3 = ((2c_3 + c_4)Tan(\pi/6)/2, c_4/2, -t),\\
&[R_6^4] = [Z(-2\pi/3)], d_6^4 = (0,0,0),\\
&[R_2^4] = [Z(2\pi/3)], d_6^4 = (0,0,0),\\
&[R_5^1] = [Y(-\gamma_1)], d_5^1 = (0,0,0),\\
&[R_5^2] = [Z(\gamma_2 + \pi/2)], d_5^2 = (0,0,0),\\
&[R_5^3] = [X(\pi/2)], d_5^3 = ((2c_3 + c_4)Tan(\pi/6)/2, -c_4/2, -t),\\
&[R_1^4] = [Z(-2\pi/3)], d_1^4 = (0,0,0),\\
&[R_3^4] = [Z(2\pi/3)], d_3^4 = (0,0,0),
\end{aligned}
\tag{11}
$$

where the special rotation angles are defined as

$$
\begin{aligned}
&\gamma_1 = \arcsin((c_4 - c_1)/2L),\\
&\gamma_2 = \arccos(H/L\cos\gamma_1).
\end{aligned}
\tag{12}
$$

By substituting the parameters in Table 1, we derived the stiffness matrix as

$$
[K] = \begin{bmatrix}
0 & 1.92E5 & 0 & 7.85E3 & 0 & 0\\
-1.92E5 & 0 & -2.91E-11 & 0 & 7.85E3 & 0\\
0 & 0 & 0 & 0 & 0 & 6.48E4\\
1.27E8 & 0 & 3.72E-9 & 0 & -1.92E5 & 0\\
0 & 1.27E8 & 0 & 1.92E5 & 0 & 0\\
3.72E-9 & 0 & 5.95E7 & 0 & 0 & 0
\end{bmatrix}. \tag{13}
$$

The compliance matrix is the inverse matrix of the stiffness matrix and it is

$$[C]=\begin{bmatrix} 0 & 1.99E-7 & 0 & 8.14E-9 & 0 & 0 \\ -1.99E-7 & 0 & 0 & 0 & 8.14E-9 & 0 \\ 0 & 0 & 0 & 0 & 0 & 1.68E-8 \\ 1.32E-4 & 0 & 0 & 0 & -1.99E-7 & 0 \\ 0 & 1.32E-4 & 0 & 1.99E-7 & 0 & 0 \\ 0 & 0 & 1.54E-5 & 0 & 0 & 0 \end{bmatrix}. \quad (14)$$

Here, we denote the loading on the top platform by a wrench,

$$\hat{\mathrm{W}}^{\mathrm{L}} = (F_x, F_y, F_z, M_x, M_y, M_z). \quad (15)$$

By Eq. (2), the deformation caused by the wrench can be derived as

$$\hat{\mathrm{T}}^{\mathrm{L}} = [C]\hat{\mathrm{W}}^{\mathrm{L}} = (\theta_x, \theta_y, \theta_z, \delta_x, \delta_y, \delta_z). \quad (16)$$

For example, when the top platform is loaded with a target sample and its weight is 1 kg, the loading wrist can be written as

$$\hat{\mathrm{W}}^{\mathrm{L}} = (0,0,-9.8,0,0,0). \quad (17)$$

From Eq. (16), the motion caused by the target sample is

$$\hat{\mathrm{T}}^{\mathrm{L}} = (0,0,0,0,0,-1.51E-4). \quad (18)$$

This means the hexapod moves 1.51E-4 mm in the opposite y direction from the original position before the hexapod is actuated by the three planar stages.

5 CONCLUSIONS

A modeling is proposed for the derivation of the 6DOF stiffness matrix of a hexapod nanopositioner with respect to the external loadings. The derivation process can be applied to the stiffness analysis of other 6DOF compliant mechanisms. By means of the Screw Theory, the topology is analyzed and the analytical model is derived based on the geometric dimensions, and material properties. This model is used for building the stiffness-based control. When combing the platform motion due to the external loading and the position control from the three actuation stages, a forward kinematic control can be derived, especially when position sensors are not available for feedback control. The model is also useful for the derivation of the allowed loading space with respect to the workspace of the hexapod nanopositioner.

REFERENCES

Brouwer, D. and Jong, B. de and Soemers, H. (2010), “Design and modeling of a six DOFs MEMS-based precision manipulator”, *Precision Engineering,* Vol. **34** (2), pp. 307–319.

Dai, J. S. (2015), “Euler–Rodrigues formula variations, quaternion conjugation and intrinsic connections”, *Mechanism and Machine Theory*, Vol. **92**, pp. 144–152.

Ji, L. and Zhu, Y. and Moheimani, S. O. R. and Yuce, M. (2010), “A micromachined 2DOF nanopositioner with integrated capacitive displacement sensor”, *Proceeding of 2010 IEEE Sensors*, pp. 1464–1467.

N. Lobontiu (2003), “Compliant mechanisms: design of flexure hinges”, *CRC Press*.

S. Awtar, A. H. Slocum, E. Sevincer (2007), “Characteristics of beam-based flexure modules”, *ASME Journal of Mechanical Design*, Vol. **129** (6), pp. 625–639.

Shi, H. (2013), “Modeling and analysis of compliant mechanisms for designing nanopositioners”, *Ph.D. dissertation, The Ohio State University*, Columbus, OH, USA.

Shi, H. and Duan, X. and Su, H.-J. (2014), “Optimization of the workspace of a MEMS hexapod nanopositioner using an adaptive genetic algorithm”, *in Robotics and Automation (ICRA), 2014 IEEE International Conference on*, Hong Kong, May 31-June 7, pp. 4043–4048.

Shi, H. and Su, H.-J. (2012), “Workspace of a flexure hexapod nanopositioner”, *in Proceedings of 2012 ASME IDETC/CIE*, Chicago, Illinois, August 12-15.

Shi, H. and Su, H.-J. and Dagalakis, N. and Kramar, J. A. (2013), “Kinematic modeling and calibration of a flexure based hexapod nanopositioner”, *Precision Engineering*, Vol. **37**(1), pp. 117 – 128.

Shi, H. and Su, H.-J. (2013), “An analytical model for calculating the workspace of a flexure hexapod nanopositioner”, *ASME Journal of Mechanisms and Robotics*, Vol. **5**(4), p. 041009.

Shi, H. and Su, H.-J. and Dagalakis, N. (2014), “A stiffness model for control and analysis of a MEMS hexapod nanopositioner”, *Mechanism and Machine Theory*, Vol. **80**, pp. 246-264.

Su, H.-J. and Shi, H. and Yu, J. (2011), “Analytical compliance analysis and synthesis of flexure mechanisms”, *in Proceedings of 2011 ASME IDETC/CIE*, Washington, DC, August 28-31.

Su, H.-J. and Shi, H. and Yu, J. (2012), “A symbolic formulation for analytical compliance analysis and synthesis of flexure mechanisms”, *ASME Journal of Mechanical Design*, Vol.**134**(5), p. 051009.

T. Wu, J. Chen, S. Chang (2008), “A six-DOF prismatic-spherical-spherical parallel compliant nanopositioner”, *IEEE Transactions on Ultrasonics, Ferroelectrics and Frequency Control,* Vol. **55** (12), pp. 2544–2551.

Venkiteswaran, V.K. and Su. H.-J. (2015), “A parameter optimization framework for determining the pseudo-rigid-body model of cantilever-beams”, *Precision Engineering*, Vol. **40**(1), 46 – 54.

Yang, S. H. and Kim, Y. and Purushotham, K. P. and Yoo, J.-M. and Choi, Y.-M. and Dagalakis, N. (2010), “AFM characterization of nanopositioner in-plane stiffnesses”*, Sensors and Actuators A: Physical, Vol.* **163** (1), pp. 383–387.

Yang, S. H. and Kim, Y.-S. and Yoo, J.-M. and Dagalakis, N. G. (2012), “Microelectromechanical systems based Stewart platform with sub-nano resolution”, *Applied Physics Letters*, Vol.**101** (6), pp. 061909.